Colloid Polym Sci (2009) 287:385–393
DOI 10.1007/s00396-008-1974-z

ORIGINAL CONTRIBUTION

Synthesis and characterization of sulfonated polymethylsiloxane polymer as template for crystal growth of $CaCO_3$

Andrónico Neira-Carrillo · Ranjith Krishna Pai · M. Soledad Fernández · Esteban Carreño · Patricio Vasquez Quitral · Jose Luis Arias

Received: 16 September 2008 / Revised: 11 November 2008 / Accepted: 22 November 2008 / Published online: 4 December 2008

Abstract The objective of this work was to synthesize a sulfonated polymethylsiloxane (S-PMS) by hydrosilylation and sulfonation reactions and to investigate their effect on the growth of $CaCO_3$ crystals using a gas diffusion method as a function of concentration, pH, and time. The result of IR and NMR shows good agreement with all proposed structures. Scanning electron microscopy images of $CaCO_3$ showed small well-defined calcite-forming short piles (ca 5 μm) and elongated calcite (ca 20 μm) crystals. The morphology of the resultant $CaCO_3$ crystals reflects the electrostatic interaction of sulfonate moieties and Ca^{2+} modulated by S-PMS adsorbed onto the $CaCO_3$ surface. X-ray diffraction confirmed the crystalline calcite polymorph. Energy dispersive spectroscopy of $CaCO_3$ crystals determined the presence of Si atoms from S-PMS. The use of PMS chemistry as an organic additive for the production of $CaCO_3$ particles is a viable approach for studying the biomineralization and could be useful for the design of novel materials with desirable shape and properties.

Keywords Polysiloxane · Hydrosilylation · Gas diffusion crystallization · Calcite · Energy dispersive spectroscopy

A. Neira-Carrillo · R. K. Pai · M. S. Fernández · E. Carreño · P. V. Quitral · J. L. Arias
Faculty of Veterinary and Animal Sciences, University of Chile, Santiago, Chile

A. Neira-Carrillo · R. K. Pai · M. S. Fernández · E. Carreño · P. V. Quitral · J. L. Arias
Center for Advanced Interdisciplinary Research in Materials (CIMAT), Santiago, Chile

A. Neira-Carrillo · R. K. Pai · M. S. Fernández · E. Carreño · P. V. Quitral · J. L. Arias
Materials Chemistry Research Group, Department of Physical, Inorganic and Structural Chemistry, Arrhenius Laboratory, Stockholm University, SE-106 91 Stockholm, Sweden

A. Neira-Carrillo (✉) · M. S. Fernández · E. Carreño · P. V. Quitral · J. L. Arias
Departamento de Ciencias Biológicas y Animales, Facultad de Ciencias Veterinarias y Pecuarias, Universidad de Chile, Santa Rosa 11735, Paradero 34, La Pintana, Santiago, Chile
e-mail: aneira@uchile.cl

R. K. Pai
Materials Chemistry Research Group, Department of Physical, Inorganic and Structural Chemistry, Arrhenius Laboratory, Stockholm University, SE-106 91 Stockholm, Sweden

Introduction

Polymethylsiloxanes (PMS) are silicone compounds that have many interesting features and which represent the most widely used silicon-based organic polymers in different applications [1, 2]. PMS are known for their useful properties such as flexibility, permeability to gases, low glass transition temperature, and low surface energy. The main synthetic route leading to functionalized PMS is the hydrosilylation of unsaturated functional compounds (allyl derivatives) with polysiloxanes containing Si-H active groups [3, 4]. This synthetic route is associated with more interesting and specific properties due to the regularly arranged functional groups on the backbone chain. There are many studies on the production of modified PMS, both medical and nonmedical application [5–9].

However, there are a few reports of the use of polysiloxane chemistry in biomineralization and very little investigation of the use of PMS for calcite nucleation [10–12]. In this context, polysiloxane membranes have demonstrated that inorganic materials might also be active in controlling crystal nucleation and growth [10, 14]. For instance, nucleation of calcite and of other calcium salts such as calcium silicate and silanolate, has been achieved in the presence of different catalysts with cross-linked poly(dimethylsiloxane) mounted on glass slides.[11] Biomineralization is a widespread phenomenon among living systems (e.g., mollusk and egg shells, crustacean carapaces, coral, bones, teeth, etc.) in which $CaCO_3$ is an important inorganic mineral [13–14]. Biomineralization has been extensively studied to investigate the control of mineralization by biological molecules and how crystal polymorph and structure can be controlled by organic additives [12, 15]. In the fabrication of hybrid inorganic–organic composites, a small amount of organic component exerts substantial control on the mineralization process [16–18]. Furthermore, the mineralization mechanism is altered by different chemical groups (e.g., amine, sulfate, and carboxylate) and functionalized networks [19–23]. Particular polyanionic sulfated macromolecules referred to as proteoglycans have been described by our group to be involved in the calcification of biominerals [24, 25]. Different approaches have been used to synthesize specific polymorphs of $CaCO_3$ in various forms such as films, spheres, sponge-like structures, ligand–receptor complexes, block copolymers and synthetic polypeptides [26–32].

Herein we report the effect of sulfonated polymethylsiloxane (S-PMS) produced by hydrosilylation and sulfonation reactions as an organic additive on crystal growth of $CaCO_3$ using a gas diffusion method [33]. We found that the spatial arrangement of sulfonate groups on S-PMS can alter $CaCO_3$ crystal nucleation, orientation, and morphology at various concentrations of S-PMS and as a function of pH and time [34]. Our work is motivated by the paucity of reports on the effect of PMS in mineralization experiments. Hence, we describe the synthesis and characterization of S-PMS and our investigation of its influence on in vitro $CaCO_3$ crystallization.

Experimental

Materials and measurements

Polymethylsiloxane, styrene, toluene, methylene chloride (CH_2Cl_2), and all solvents were dried and distilled under argon. CH_2Cl_2 was purified by refluxing over lithium aluminum hydride for 72 h. The 2-propanol and sulfuric acid (95–97%) were used without further purification. The dicyclopentadienyl platinum (II) chloride (Cp_2PtCl_2) catalyst used for the hydrosilylation reaction was synthesized from hydrated hexachloroplatinic acid (IV) and diclyclopentadiene respectively [35].

IR spectra were obtained on Perkin Elmer Paragon 1000 and Bruker Vector 22 instruments. NMR (^1H, ^{13}C, ^{29}Si) of the functionalized PMS (F-PMS) and sulfonated PMS (S-PMS) were obtained with a Bruker 250 MHz and AMX 300 MHz (Fig. 1). The molecular weight (MW) determination was carried out by using PSS-Win GPC-PSS gel permeation chromatography (GPC). The $CaCO_3$ crystals formed after in vitro crystallization were collected and then coated with gold on an automated sputter coater

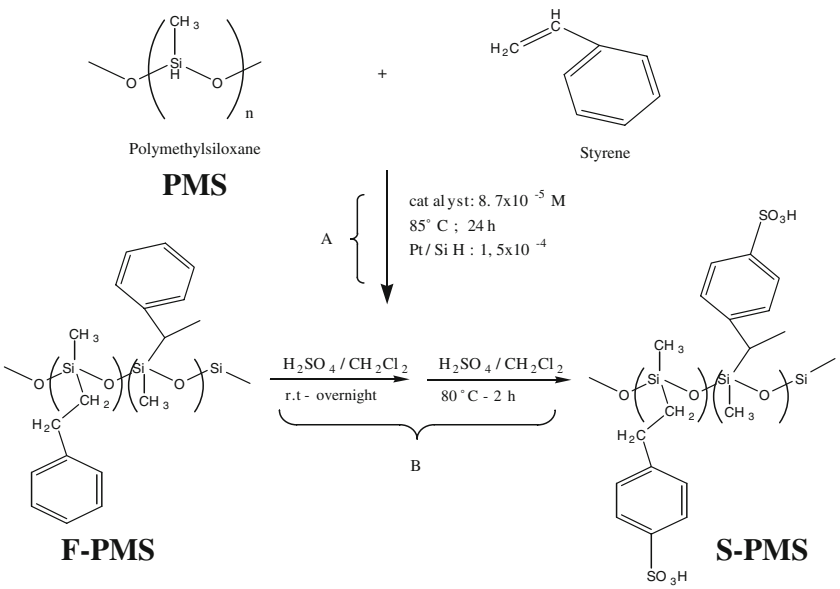

Fig. 1 Synthesis of F-PMS and S-PMS after the **a** hydrosilylation and **b** the sulfonation reactions

(EMS-550). For scanning electron microscopy (SEM) and energy dispersive X-ray (EDS) analysis, the $CaCO_3$ crystals were examined with a Tesla BS 343A and JEOL JSM-5410 at 15 kV, respectively. The diffraction spectra were taken from a powdered sample on a paper filter supported on a metal base in a Siemens D-5000 X-ray diffractometer with CuK_α radiation (graphite monochromator). The geometric scanning Bragg–Brentano (θ–θ) and the angle range from 5° to 70° (2θ) were performed. The filter used as a support was a Gelman Sciences Sepraphore III membrane [36]. The Diffrac Plus was used as data control software.

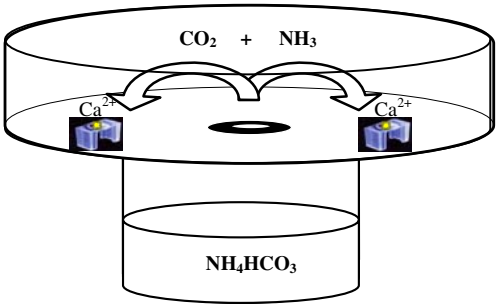

Fig. 2 Schematic representation of the experimental setup for the gas diffusion method

Hydrosilylation and sulfonation reactions

The hydrosilylation reaction of PMS was done with styrene as unsaturated compound and Cp_2PtCl_2 as catalyst [36, 37]. Briefly, styrene (15 mol% excess versus the Si–H of PMS) was dissolved in 100 ml of sodium-dried, freshly distilled toluene together with the stoichiometric amount of PMS. The reaction mixture was heated to 85 °C under argon, and 100 μl of Cp_2PtCl_2 as a solution in CH_2Cl_2 was then injected. The mole ratio of Pt/SiH catalyst was 1.5×10^{-4}. The mixture was refluxed under argon with agitation until both IR and ^1H NMR showed that the hydrosilylation reaction was complete. Then, the F-PMS was dried under vacuum at 40°C for 72 h. The yield from the hydrosilylation was 95%. The S-PMS was prepared by dissolving the F-PMS in CH_2Cl_2 with a stoichiometric amount of sulfuric acid overnight at room temperature after which the reaction temperature was increased to 80 °C, and the mixture was incubated for 2 h. Then, the mixture was evaporated, and the S-PMS was washed and dried under vacuum at 40 °C for 2 h. The yield from the sulfonation was 98%.

Crystallization method

Calcium chloride ($CaCl_2$), ethanol, and tris(hydroxymethyl) aminomethane (TRIS) were obtained from ACS-Merck, and ammonium hydrogen carbonate (NH_4HCO_3) was from J.T. Baker. All reagents were of the highest available grades. Deionized water was obtained from capsule filter 0.2 μm flow (U.S. Filter). The $CaCO_3$ crystallization was based on the gas diffusion method (Fig. 2) and carried out as described elsewhere [24, 38–40]. The gas diffusion method was performed using a chamber consisting of a 85-mm plastic Petri dish having a central hole in its bottom which is glued to a plastic cylindrical vessel. Inside the chamber, polystyrene microbridges were filled with 35 μl of 200 mM $CaCl_2$ solution in 200 mM TRIS buffer. The cylindrical vessel contained 3 mL of 25 mM NH_4HCO_3 solution. All experiments were carried out inside the Petri dish using S-PMS polymer at different concentrations (32, 64, and 1.6 mg/mL) at 20 °C for 24 h. For these experiments, a stock solution of 1.6 mg of S-PMS in deionized water at different pH (from 7 to 12) was prepared as mother solution in an Eppendorf tube. All experiments were carried out inside the Petri dish using different pH, from 7 to 12, at 20 °C for 24 h. A microbridge was filled with a 35-μl of $CaCl_2$ solution without additive as blank control and one with PMS as a negative control. All crystals of $CaCO_3$ result from the diffusion of carbon dioxide (CO_2) gas into the buffered $CaCl_2$ solution. The crystallization occurs on the surface of the filter paper in which the polymer was deposited first. The microbridges with the $CaCO_3$ crystals formed were carefully rinsed with deionized water and dehydrated through solution of ethanol in growing concentrations (50%, 80%, and 100%), dried at room temperature, and observed the microstructure by SEM. The pH is very important in the biomineralization field. In gas diffusion method, the $CaCO_3$ crystallization is performed at 24 h, and the effect of pH is eliminated by fixing the pH using TRIS buffer.

Results and discussion

The term hydrosilylation describes an addition reaction in which compounds with one or more Si–H bonds combine with any reagent [4]. The hydrosilylation reaction of PMS was monitored with IR and NMR techniques by the decrease of the Si–H bond. Figure 3 represents the IR spectra of PMS, F-PMS, and S-PMS polymers. Figure 3a shows a classic organosilicon IR spectrum in which the most typical absorption peaks are at 2,157 cm^{-1} and around 1,222–966 cm^{-1} due to Si–H and Si–O–Si bonds, respectively [41, 42]. In Fig. 3b, the absorption peak of Si–H has disappeared demonstrating that the hydrosilylation was complete. The broad absorption bands at 3,000 cm^{-1} are assignable to the incorporation of carbon/hydrogen bonds on the main chain of F-PMS and S-PMS. The absorption bands of Si–O–Si and Si–CH_3 were also found. Figure 3c

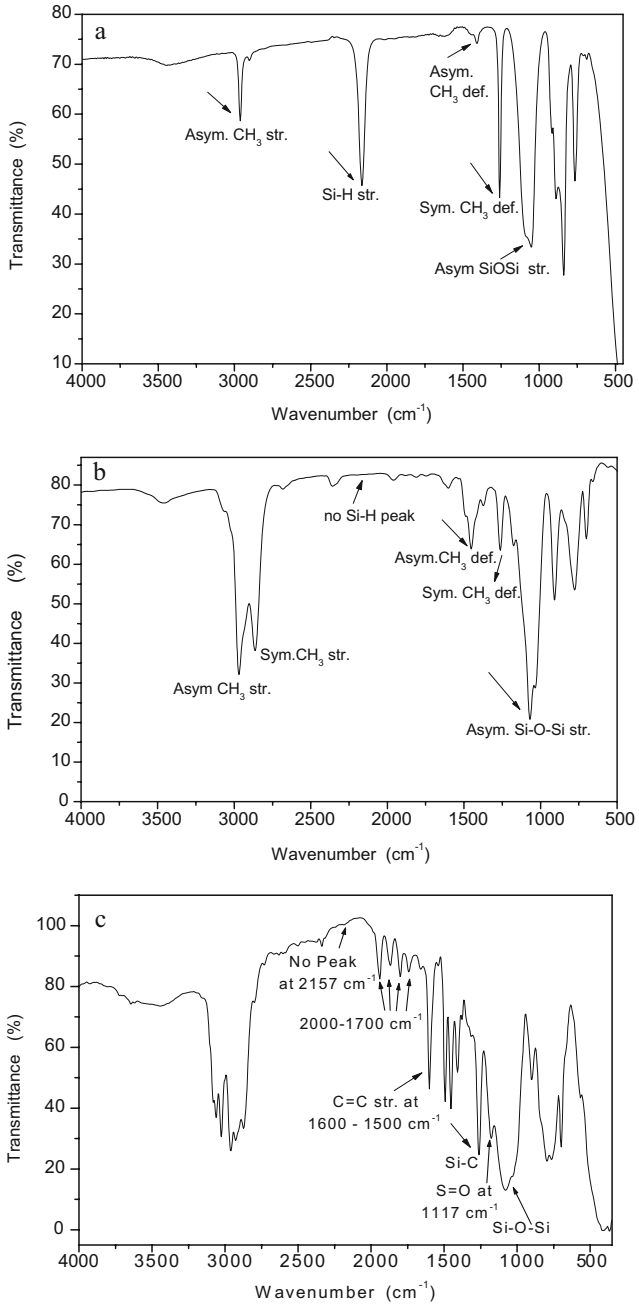

Fig. 3 IR of **a** PMS, **b** F- PMS, and **c** S-PMS

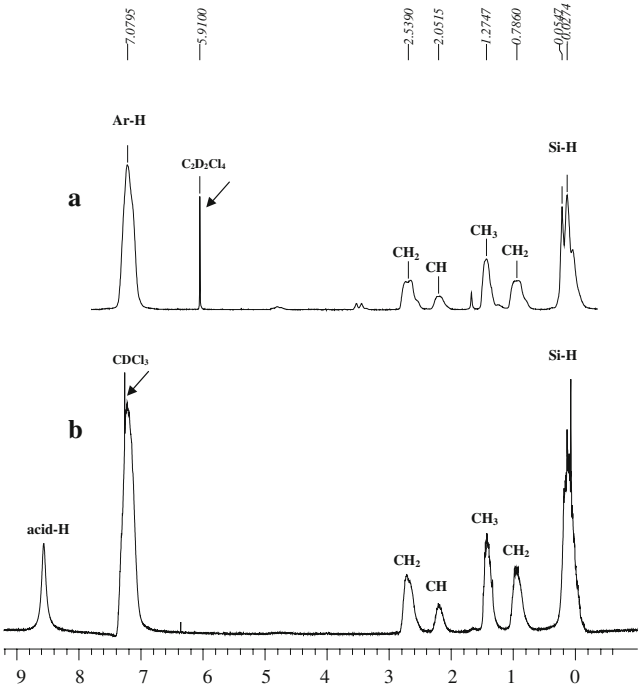

Fig. 4 ^{1}H-NMR of **a** F-PMS and **b** S-PMS. The $C_2D_2Cl_4$ and $CDCl_3$ were used as deuterated solvents

shows the C=C stretching absorptions of an aromatic compound around 1,600 and/or 1,500 cm^{-1} with four absorption bands between 2,000 and 1,700 cm^{-1}, which indicates the mono substitution of an aromatic ring. The S=O stretching absorption occurs at 1,215 and 1,010 cm^{-1}. All the absorption peaks obtained by IR are in good agreement with the chemical structures of PMS, F-PMS, and S-PMS [34].

Figure 4 shows the NMR spectra of F-PMS (Fig. 4a) and S-PMS (Fig. 4b) obtained after hydrosilylation and sulfonation reactions, respectively. In Fig. 4(a) the different proton signals at $\delta \sim 0.78$ and $\delta \sim 2.3$ ppm can be assigned to $-CH_2$, and the signals at $\delta \sim 1.27$ and $\delta \sim 2.05$ ppm are due to $-CH_3$ and –CH, respectively. The aromatic protons from styrene were determined as an intense singlet at $\delta \sim 7.0$ ppm in both spectra. These broad but well resolved signals presumably are due to the high of MW and polydispersity (D) values of F-PMS despite the flexible polymer backbone. The MW of F-PMS was 1.5×10^4 (g/mol) and its polydispersity (D=2.7) was determined by GPC. Nevertheless, the ^{1}H-NMR of S-PMS (Fig. 4) showed an extra peak at 8.5 ppm which is attributed to the sulfonate group inserted on the aromatic ring of F-PMS.

In order to evaluate the effect of sulfonate moieties of the S-PMS as an organic additive on in vitro $CaCO_3$ mineralization, a set of $CaCO_3$ crystallization experiments was performed with S-PMS as a soluble additive and/or gel substrate, and the morphology of the resultant $CaCO_3$ crystals was investigated. The in vitro $CaCO_3$ crystallization was carried out with a gas diffusion method by varying the concentration, pH, and time at 20 °C. Figure 5 shows the SEM images of $CaCO_3$ crystals grown in the presence of different S-PMS concentrations at 20 °C at pH 9 for 24 h. Figure 5a shows the typical morphology of rhombohedral calcite crystals obtained without additive, and in Fig. 5b, we observed similar rhombohedral morphology in the presence of PMS without sulfonate moieties as negative control. The $CaCO_3$ obtained with different concentrations of S-PMS resulted in modified calcite crystals in the size range between 10 and 25 μm. For

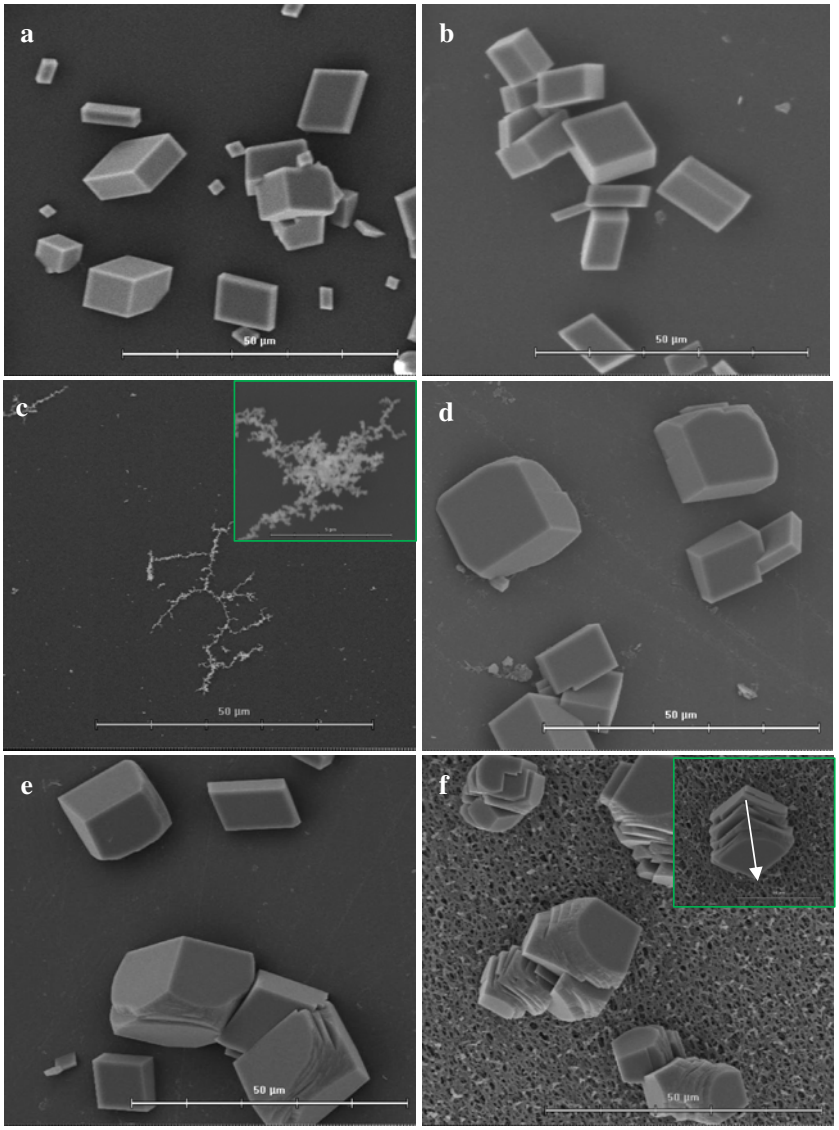

Fig. 5 SEM of $CaCO_3$ crystals obtained in the presence of PMS and S-PMS at 20 °C at pH 9 for 24 h: **a** control calcite, **b** calcite obtained with PMS, **c** 64 µg (substrate) of S-PMS, **d** 32 µg/ml of S-PMS, **e** 64 µg/ml of S-PMS, and **f** 1.6 mg/ml of S-PMS

instance, Fig. 5c shows $CaCO_3$ crystals obtained with S-PMS (64 µg) as a substrate, which revealed a highly electrostatic interaction of sulfonate groups with Ca^{2+} ion inducing a selective deposition of $CaCO_3$ in a network consisting of S-PMS chains bridged by Ca^{2+}. Crystallization of inorganic materials on solid templates has attracted a great deal of attention showing significant effects on the control of $CaCO_3$ crystallization. It is known that PMS have a much higher permeability to gases than other synthetic polymers which can be useful in the gas diffusion method. This phenomenon is due to the torsion and bending flexibility of S-PMS, which elicits a characteristic nucleation and growth of $CaCO_3$ crystals. Similar results have been reported with sulfonic acid-based hydrogels in a polyacrylamide network [34] using double-diffusion crystallization and with polycarboxylate polymers as an additive [43, 44]. Furthermore, Fig. 5d–f shows the $CaCO_3$ crystal morphologies obtained with 32, 64 and 1.6 mg/ml of S-PMS as additive during crystallization at pH 9. At a lower concentration of S-PMS, 10 to 20 µm size and modified calcite crystals were obtained (Fig. 5d,e). However, when the concentration of S-PMS is increased (Fig. 5f), no single rhombohedral calcite crystals were found, and only aggregated calcite crystals elongated along the crystallographic *c*-axis direction were observed on the filter paper background. The white arrow shows the *c*-axis for the calcite crystals. Closer examination of these elongated calcites revealed that they have smooth surfaces and poorly defined end faces, and all the single crystals lost their well-defined rhombohedral shape (Fig. 5f, insert). The size of these crystals was between 15 and 25 µm. Clearly at a high concentration (1.6 mg/ml), the S-PMS exerted a strong inhibitory effect on growing rhombohedral calcite, and we found very few single crystals, which demonstrate the robust inhibitory nucleation properties of S-PMS during $CaCO_3$ crystallization. We believe that the aggregation

process of the truncated calcite crystals occur due to nonspecific adsorption of the charged sulfonate moieties of S-PMS onto the crystal faces, which blocks specific growth directions. Face selective nucleation of $CaCO_3$ crystals has been clearly demonstrated with self-assembled monolayers [45] and by varying the carboxylate content of functionalized polymers [46, 47]. On the other hand, it has been described that the presence of sulfate moieties of sulfate glycoaminoglycans (GAGs) makes it possible to control the nucleation and produce drastic modification of $CaCO_3$ morphology [25, 34].

For evaluating the influence of the pH and time of crystallization of the sulfonate groups of S-PMS, a set of $CaCO_3$ crystallization experiments was carried out by altering the pH (in the range of 7–12) and time (1, 6, and 24 h) at a constant concentration of S-PMS at 20 °C. Figure 6a–f shows the effect on $CaCO_3$ crystal morphology obtained with S-PMS at 1.6 mg/ml for 1 h at pH in the range of 7 to 12. Different morphologies of $CaCO_3$ crystals were only obtained for pH 8 to 12 (Fig. 6b–f), and no crystals were observed at pH 7 (Fig. 6a). Figure 6b shows precursor nanoparticles of $CaCO_3$ granules (ca 500 nm in size) at pH 8. Figure 6c–f shows $CaCO_3$ crystals obtained at pH 9 to 12. These aggregated crystals lost their well-developed edges and show elongation on the atomic steps on the (104) face. Figure 6f shows a number of very small aggregated rhombohedral calcite crystals forming short piles (5 μm in size) obtained at pH 12. A similar calcite crystal morphology with a stairstep dendritic structure has been reported with synthetic peptides and synthetic organic polymer like poly (vinyl alcohol) [48, 49].

When the same set of $CaCO_3$ crystallization experiments was carried out for 6 and 24 h, a similar tendency was found; however, in this experiment, the nucleation of precursor nanoparticles of $CaCO_3$ occurred at lower pH. As shown in Fig. 7a, at pH 7, there are numerous precursor nanoparticles of $CaCO_3$ granules on the filter surface. Figure 7a–f shows the resultant $CaCO_3$ crystals obtained at pH 7 to 12 for 24 h. Figure 7c–f shows aggregated crystals obtained at pH 8 to 12. Figure 7e and f show elongated $CaCO_3$ crystals (Fig. 8) forming piles in the range of 10–30 μm in size. We observed that the surface of the background filter paper was smoother without any precursor nanoparticles (Fig. 7d–f) indicating precursor particles start to dissolve due to higher ionization degree of the template. Under such condition, there is drastic increase in the supersaturation level of Ca^{+2} which exceeds the solubility limit, and hence, compact piles of $CaCO_3$ crystals is nucleated from the solution. Here, we assume that the accumulation of Ca^{2+} ions are better at pH 12 due to ionization and of the expected spatial arrangement of sulfonate groups of S-PMS, which facilitates interaction between Ca^{2+} ions and sulfonate groups during $CaCO_3$ crystallization. It is known that dissolution–crystallization phenomenon is related to the critical polymer concentration needed for the stabilized nanoparticle precursor of $CaCO_3$ granules and with the concept that stereochemical interactions of an organic acid and Ca^{2+} provide the morphogenetic and orientation control of $CaCO_3$ biogenic crystals [34, 43, 45, 50, 51].

Taking this into account, we suspect that the S-PMS polymer is adsorbed on the $CaCO_3$ surface, and the

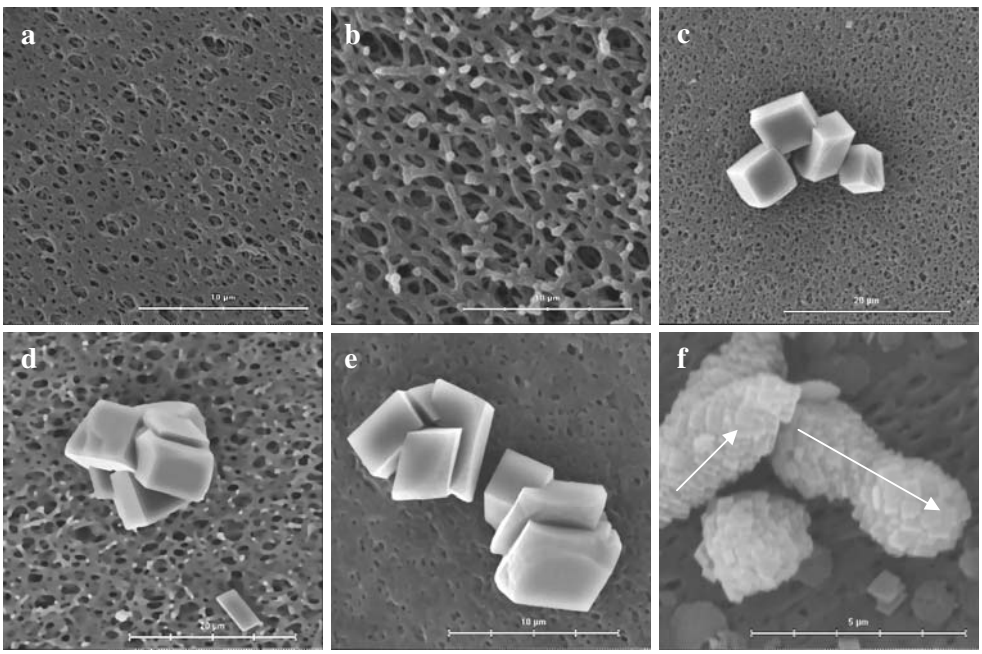

Fig. 6 SEM of $CaCO_3$ crystals obtained in the presence of S-PMS at 20 °C for 1 h. **a** pH 7, **b** pH 8, **c** pH 9, **d** pH 10, **e** pH 11, and **f** pH 12

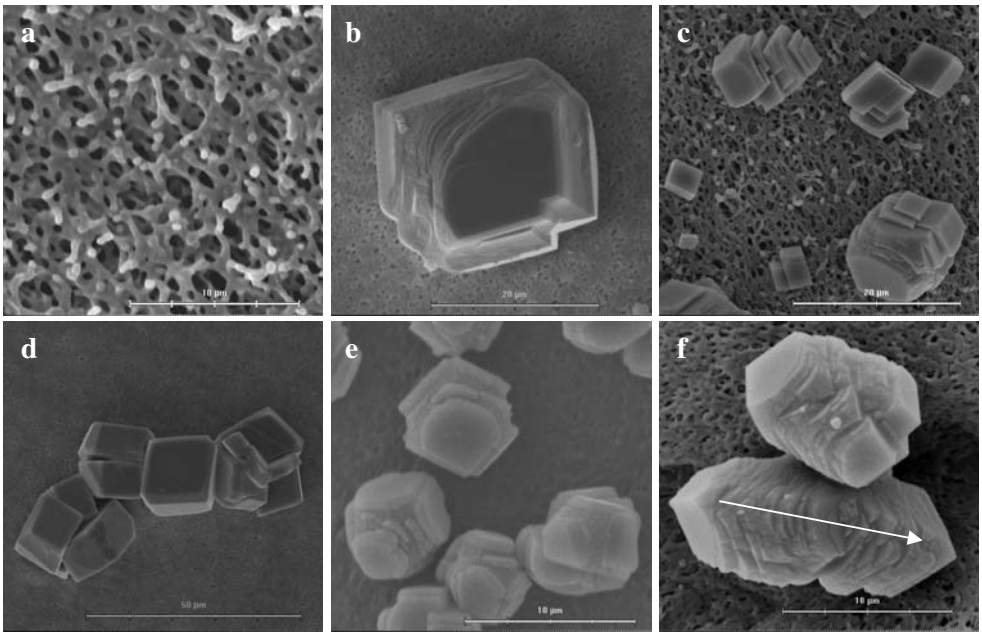

Fig. 7 SEM of $CaCO_3$ crystals obtained in the presence of S-PMS at 20 °C for 24 h. **a** pH 7, **b** pH 8, **c** pH 9, **d** pH 10, **e** pH 11, and **f** pH 12

presence of the sulfonate moieties bonded to the polymer backbone produce a local Ca^{2+} ion accumulation, which is more pronounced at higher pH. The stereochemical interaction of the S-PMS with the $CaCO_3$ surface and subsequently growth of crystals by blocking the facets can be visualized in the follow scheme.

The effects of temperature and pressure on the nucleation of $CaCO_3$ are most important parameters in order to obtain less thermodynamic polymorphs. There are several reports on the effects of lower temperature on the nucleation of calcium carbonate. For example, the presence of additives like aspartic acid immobilized polyacrylic acid (PA-Asp) induced the nucleation of spherical vaterite polymorph at 4 °C. However, at room temperature, a thin film of calcite was deposited. Moreover, stable amorphous $CaCO_3$ was precipitated in the presence of Mg at low temperature. Valiyaveettil et al. reported that at low temperature the presence of additives influence the nucleation, polymorph selectivity, and morphology of the precipitated $CaCO_3$ particles [52]. Nevertheless, the scope of the current study was to demonstrate the influence of S-PMS on the $CaCO_3$ crystallization behavior using gas diffusion method by varying only two parameters, say polymer concentration and pH. The temperature is crucial in order to study the polymorphs of $CaCO_3$ [53], whereas we believe that the mechanism and kinetics of crystallization are strongly influenced by the solubility and charge density behavior of polymer in aqueous solution.

EDS analysis was carried out in order to investigate the presence of Si on the $CaCO_3$ crystals. EDS measurements of $CaCO_3$ crystals obtained at pH 9 for 24 h (Fig. 9a,b) and pH 12 (data no shown) detected different elemental compositions of Si adsorbed on the elongated calcite crystals, which demonstrates the strong inhibitory properties of S-PMS. A small amount of Si from S-PMS on the surface, in the range of 0.94% (at pH 9) and of 1.61% (at pH 12) was necessary to modified $CaCO_3$ crystals. The Si percentage was higher in between the crystal surfaces than at the bottom or lateral positions. It is important to mention that the amount of Si from S-PMS detected here is in agreement with the organic matrix content found in nature, which indicates that morphogenetic aspect of this inorganic material can be well controlled by a small amount of S-PMS as an additive [10, 12–14, 50]. Figure 9b shows the SEM image and the screening of Si and Ca atoms over a short distance (about 20 μm) at pH 9. Although the EDS technique is a surface technique, and it is difficult to do quantitative determinations, this screening showed no constant distribution of Ca and Si elements. This observation provides evidence that the Ca^{2+} concentration on the $CaCO_3$ surface is regulated by the

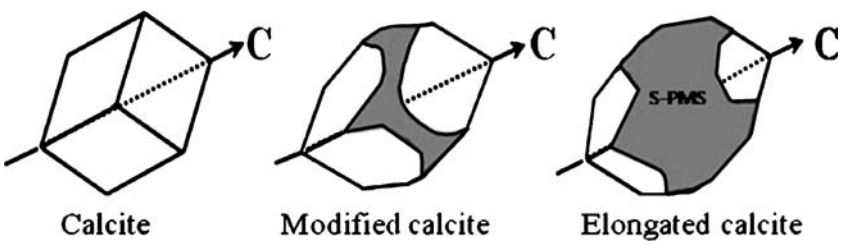

Fig. 8 Representation of $CaCO_3$ crystals elongation in the presence of S-PMS

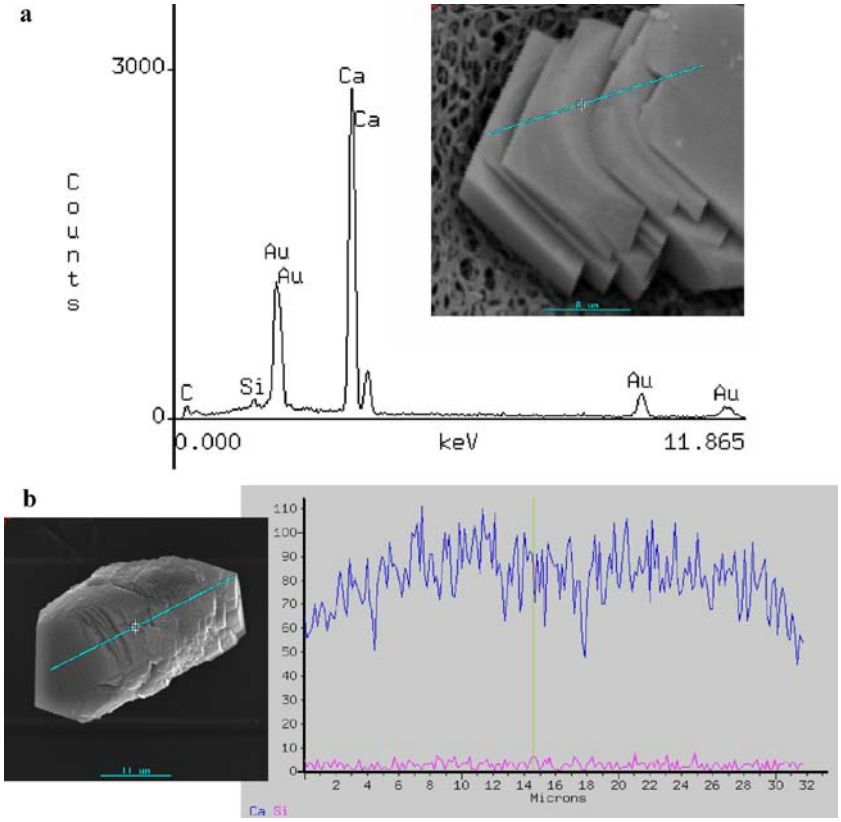

Fig. 9 EDS and screening of Si and Ca atoms of $CaCO_3$ obtained in the presence of S-PMS for 24 h at 1.6 mg/ml. **a** EDS at pH 9, **b** screening of Si (*pink color*) and Ca (*blue color*) atoms

distribution of Si from S-PMS. We suspect that the variation of the Ca^{2+} content could be regulated by the adsorption of Si from S-PMS. On the other hand, we observed $CaCO_3$ crystals grown in the bottom of the microbridges with similar crystal morphology due to the diffusion of S-PMS molecules from the filter into the solution with higher concentration of Si (1.74%).

Figure 10 shows the XRD patterns of the $CaCO_3$ crystals grown in the presence of S-PMS. It can be seen that the strongest diffraction intensity are the peaks around $2\theta=50.0°$ and $2\theta=43.0°$, which are due to the metal base (copper) and the peaks around $2\theta=13–24°$ are ascribed to the diffraction of the filter. This XRD patterns shows the crystalline peak at $2\theta=29.6°$ confirming the polymorphism of calcite.

Conclusions

The presence of S-PMS can effectively control the morphogenesis and the crystallographic polymorphism of $CaCO_3$ crystals. Concentration of S-PMS, pH, and time were found to be crucial during $CaCO_3$ nucleation and growth. At different pH, S-PMS can undergo changes in charge of the sulfonate groups and adopt different orientations in solution and thereby elicit changes in $CaCO_3$ morphology. We surmise that the crystallization of calcite, which is triggered by the sulfonate groups of S-PMS results from a local accumulation of Ca^{2+} ions, which correlates closely with the polymer's nature, concentration, pH, and crystallization time [33]. The similarity in $CaCO_3$ morphology observed on the bottom of the microbridges is explained by diffusion of S-PMS. IR and NMR analysis are in good agreement with the proposed F-PMS and S-PMS structures. SEM analysis showed different $CaCO_3$ crystal morphology as a function of pH from precursors of $CaCO_3$ nanoparticles to

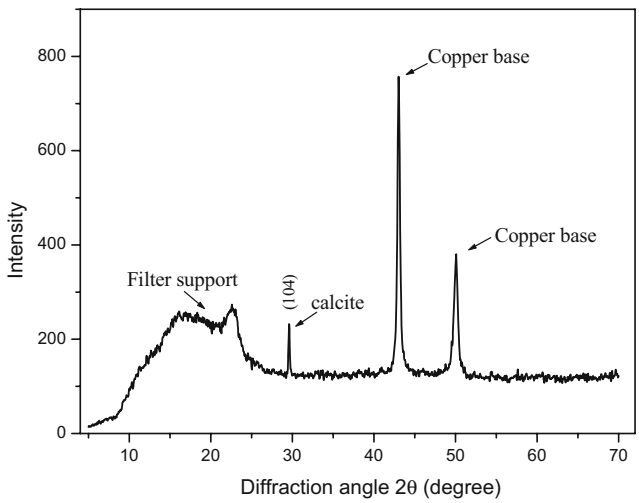

Fig. 10 XRD patterns of $CaCO_3$ crystals grown in the presence of S-PMS

aggregated calcite crystals occurring as short piles (5 μm) and elongated calcite crystals (20 μm). EDS revealed the presence of Si from S-PMS adsorbed onto the modified $CaCO_3$ crystals and XRD demonstrated calcite polymorph. In summary, we demonstrated that the use of PMS chemistry as an additive or substrate templates [34, 54, 55] provides a viable approach for studying various aspects of biomineralization including production of controlled particles, polymorphism, and defined morphologies.

Acknowledgements This research was supported by FONDECYT 11070136 and FONDAP 11980002 granted by the Chilean Council for Science and Technology (CONICYT), and partially by Fundación Andes C-1406031.

References

1. Brook MA (2000) Silicon in Organic, Organometallic, and polymer Chemistry, Ed. Wiley, INC
2. Abe Y, Gunji T (2004) Prog Polym Sci 29:149
3. Ojima I (1989) The Hydrosilylation Reaction: The Chemistry of Organic Silicon Compounds, Ed. by S. Patai, et al.
4. Speier LJ (1979) Homogeneous Catalysis of Hydrosilation by Transition Metals. Adv Org Chem
5. Kaneko Y, Sato S, Kadokawa J-I, Iyi NJ (2006) Mater Chem 16:1746
6. Lee S, Vörös J (2005) Langmuir 21:11957
7. Zhang XD, Macosko CW, Davis HT, Nikolov AD, Wasan DT (1999) J Colloid Interf Sci 215:270
8. Hu S, Ren X, Bachman M, Sims CE, Li GP, Allbritton NL (2004) Langmuir 20:5569
9. Sia SK, Whitesides GM (2003) Electrophoresis 24:3563
10. Brisdon BJ, Heywood BR, Hodson AGW, Mann S, Wong KKW (1993) Adv Mater 5:49
11. Wong KKW, Brisdon BJ, Heywood BR, Hodson AGW, Mann S (1994) J Mater Chem 4:1387
12. Meldrum FC (2003) Int Mater Rev 48:187
13. Lowenstam HA, Weiner S (1989) On biomineralization. Oxford Univ. Press, UK
14. Mann S (2001) Biomineralization: principles and concepts in bioinorganic materials chemistry. Oxford Univ. Press, Oxford
15. Cölfen H (2003) Curr Opin Colloid Interf Sci 8:23
16. Weiner S, Addadi L (1997) J Mater Chem 7:689
17. Cölfen H, Mann S (2003) Angew Chem Int Ed 42:2350
18. Nys Y, Hincke MT, Arias JL, Garcia-Ruiz JM, Solomon SE (1999) Poultry Avian Biol Rev 10:142
19. Grassmann O, Lobmann P (2004) Biomaterials 25:277
20. Weissbuch I, Addadi L, Lahav M, Leiserowitz L (1991) Science 253:637
21. Aizenberg J (2000) J Cryst Growth 211:143
22. Pai RK, Hild S, Ziegler A, Marti O (2004) Langmuir 20:3123
23. Addadi L, Moradian J, Shay E, Maroudas NG, Weiner S (1987) Biophysics 84:2732
24. Arias JL, Fernández MS (2003) Mater Charac 50:189
25. Arias JL, Neira-Carrillo A, Arias JI, Escobar C, Bodero M, David M, Fernandez MS (2004) J Mater Chem 14:2154
26. Kato T (2000) Adv Mater 12:1543
27. Walsh D, Mann S (1995) Nature 377:320
28. Walsh D, Lebeau B, Mann S (1999) Adv Mater 11:324
29. Pai RK, Pillai S (2007) Cryst Growth Des 7:215
30. Cölfen H, Qi LM (2001) Chem Eur J 7:106
31. Neira-Carrillo A, Yazdani-Pedram M, Retuert J, Diaz-Dosque M, Gallois S, Arias JL (2005) J Colloid Interf Sci 286:134
32. Cölfen H, Mann S (2004) J Mater Chem 14:2269
33. Dominguez-Vera JM, Gautron J, Garcia-Ruiz JM, Nys Y (2000) Poultry Sci 79:901
34. Grassmann O, Lobmann P (2003) Chem-A Eur J 9:1310
35. Neira-Carrillo A (2003) PhD Thesis. University of Concepción
36. Neira-Carrillo A, Pai RK, Fuenzalida VM, Fernández MS, Retuert J, Arias JL (2008) J Chil Chem Soc 53:1469
37. Apfel MA, Finkelmann H, Janini GM, Laub RJ, Lühmann B-H, Price A, Roberts WL, Shaw TJ, Smith CA (1985) Anal Chem 57:652
38. Arias JI, Jure C, Wiff JP, Fernández MS, Fuenzalida V, Arias JL (2002) Mat Res Soc Proc 711:243
39. Neira-Carrillo A, Fernández MS, Retuert J, Arias JL (2003) Mat Res Soc Proc EXS-1:321
40. Fernández MS, Passalacqua K, Arias JL (2004) J Struct Biol 148:1
41. Pouchert JC (1975) The Aldrich Library of Infrared Spectra. Aldrich Chemical Company, INC
42. Rodríguez-Baeza M, Neira CA, Aguilera JC (2003) J Chil Chem Soc 48:72
43. Rieger J, Thieme J, Schmidt C (2000) Langmuir 16:8300
44. Rieger J, Hädicke E, Rau IU, Boeckh D (1997) Tenside Surfactants Deterg 34:430
45. Han YJ, Aizenberg J (2003) Angew Chem Int Ed 42:3668
46. Aizenberg J, Black AJ, Whitesides GM (1999) J Am Chem Soc 121:4500
47. Roqué J, Molera J, Vendrell-Saz M, Salvadó N (2004) J Cryst Growth 262:543
48. Kim IW, DiMasi E, Evans JS (2004) Cryst Growth Des 4:1113
49. Kim W, Robertson RE, Zand R (2005) Cryst Growth Des 5:513
50. Dove PM, DeYoreo JJ, Weiner S (2003) Biomineralization, Vol. 54 of Reviews in Mineralogy and Geochemistry. Mineralogical Society of America
51. Xu AW, Ma Y, Cölfen H (2007) J Mater Chem 17:415
52. Sindhu S, Ajikumar PK, Jegadesan S, Valiyaveettil S (2004) Mat Res Soc Proc MRS, Paper EE9.3853
53. Wang C, Zhao J, Zhao X, Bala H, Wang Z (2006) Powder Technol 163:134
54. Li H, Estroff LA (2007) J Am Chem Soc 129:5480
55. Petrova RI, Swift JA (2004) J Am Chem Soc 126:1168